The Astrophysical Journal, 1005:89 (15pp), 2026 July 1 https://doi.org/10.3847/1538-4357/ae6f08

A Systematic NLTE Study of Very Metal-poor Stars with Metallicity Down to −4.3 dex. II. Lithium Abundance and New Insight of the Lithium Plateau

Hong-Liang Yan[1,2,3], Jinxiao Qin[1,2,4], Shuai Liu[1], Zeming Zhou[1], Gang Zhao[1,3], Jianrong Shi[1], Sofya Alexeeva[1], Huawei Zhang[5,6], Haining Li[1], Huiling Chen[5,6], Junbo Zhang[1], Yufu Shen[7], Wako Aoki[8,9], Tadafumi Matsuno[10], and Jingkun Zhao[1]

[1] National Astronomical Observatories, Chinese Academy of Sciences, Beijing 100101, People's Republic of China; hlyan@nao.cas.cn, gzhao@nao.cas.cn
[2] Institute for Frontiers in Astronomy and Astrophysics, Beijing Normal University, Beijing 102206, People's Republic of China
[3] School of Astronomy and Space Science, University of Chinese Academy of Sciences, Beijing 100049, People's Republic of China
[4] Department of Physics, Hebei Normal University, Shijiazhuang 050024, People's Republic of China
[5] Department of Astronomy, School of Physics, Peking University, Beijing 100871, People's Republic of China
[6] Kavli Institute of Astronomy and Astrophysics, Peking University, Beijing 100871, People's Republic of China
[7] Changchun Observatory, National Astronomical Observatories, Chinese Academy of Sciences, Jingyuetan National Scenic Area, Changchun 130117, People's Republic of China
[8] National Astronomical Observatory of Japan, 2-21-1 Osawa, Mitaka, Tokyo 181-8588, Japan
[9] Astronomical Science Program, The Graduate University for Advanced Studies, SOKENDAI, 2-21-1 Osawa, Mitaka, Tokyo 181-8588, Japan
[10] Astronomisches Rechen-Institut, Zentrum für Astronomie der Universität Heidelberg, Mönchhofstraße 12-14, 69120 Heidelberg, Germany
Received 2025 October 22; revised 2026 May 15; accepted 2026 May 15; published 2026 June 26

Abstract

Metal-poor stars are crucially important for understanding the early Galaxy, first stars, and the Universe. In this series of papers, we present a homogeneous non–local thermodynamic equilibrium (NLTE) abundance analysis of 12 elements for 103 very metal-poor (VMP)/extremely metal-poor (EMP) stars with metallicity down to −4.3 dex. The sample was selected from the LAMOST survey and observed by the high-resolution spectroscopy of Subaru. In this paper, we present the NLTE abundances and evolution of lithium in these stars. We report different lithium behaviors corresponding to different evolutionary stages and their signatures: (1) The Spite plateau shows a slightly positive slope, indicating increasing lithium abundance with increasing metallicity. Most significantly, it appears to extend to lower metallicities as previously suggested, calling into question the reality of the so-called "meltdown" at low metallicity; (2) we confirm a lithium plateau for lower red giant branch (LRGB) stars with A(Li) = 1.13 dex in our sample, while the lithium abundance drops rapidly to A(Li) < 0.5 as stars continue to evolve to a higher stage. (3) We identify four Li-rich stars in our sample across different evolutionary stages, showing complex and multiple lithium production mechanisms in VMP/EMP stars. These findings suggest that early Galactic lithium enrichment results from a complex interplay between depletion and production processes.

Unified Astronomy Thesaurus concepts: Chemical abundances (224); Stellar abundances (1577); Galaxy chemical evolution (580); Population II stars (1284); Field stars (2103)

1. Introduction

Metal-poor stars[11] are crucial for understanding the earliest epochs of the Galaxy and the Universe. Their chemical composition offers the signatures of early generation (i.e., Population III) stars, first supernovae, and interstellar medium of the proto-Galaxy (T. C. Beers & N. Christlieb 2005; K. Nomoto et al. 2013; A. Frebel & J. E. Norris 2015; T. Hartwig et al. 2019). Moreover, their spatial and kinematic properties provide insight into the hierarchical assembly of the Milky Way halo, revealing remnants of accreted dwarf galaxies and ancient stellar streams (A. Helmi et al. 2018; G. C. Myeong et al. 2018).

Systematic efforts over time have yielded increasingly robust abundance determinations for metal-poor stars (e.g., R. Cayrel et al. 2004; J. G. Cohen et al. 2013; T. Hansen et al. 2014; T. Sitnova et al. 2015; G. Zhao et al. 2016; P. François et al. 2020; W. Aoki et al. 2022; H. Li et al. 2022), and a comprehensive overview of these advances and additional references can be found in P. Bonifacio et al. (2025). Together with stars in the metal-rich end, stellar abundances across a wide metallicity range are being investigated and compared with the Galactic chemical evolution (GCE) models (e.g., D. Romano et al. 2010; C. Kobayashi et al. 2020), providing insights into the roles of different nucleosynthesis channels (S. E. Woosley & T. A. Weaver 1995), and challenging monolithic scenarios as well (e.g., W. Aoki et al. 2018; P. Bonifacio et al. 2018).

Among all the elements studied in metal-poor stars, lithium is uniquely important. ^{7}Li was initially synthesized in Big Bang nucleosynthesis (BBN). According to standard BBN theory, the primordial lithium abundance is determined by the baryon-to-photon ratio, η. Since the photon density is precisely determined by the present-day cosmic microwave background (CMB) radiation, the critical parameter is the baryon density, which can be inferred not only from CMB

[11] Based on their iron deficiency, metal-poor stars are commonly classified as metal-poor, VMP, EMP, and ultra-metal-poor (UMP) stars, etc. For convenience, we refer to our sample stars as VMP stars, although their metallicities span the range from metal poor to extremely metal poor.

anisotropies (e.g., Wilkinson Microwave Anisotropy Probe and Planck, $\Omega_b h^2 = 0.02225 \pm 0.00016$, Planck Collaboration et al. 2016) but also independently from measurements of primordial deuterium (R. J. Cooke et al. 2018), both of which provide consistent constraints. This theoretical expectation, however, stands in persistent tension with the so-called "Li plateau" or "Spite plateau" (F. Spite & M. Spite 1982a; M. Spite & F. Spite 1982b), which refers to a roughly constant lithium abundance observed in warm metal-poor ([Fe/H] < -1.5) dwarf stars, regardless of metallicity or temperature. The Spite plateau was initially interpreted as direct evidence of primordial lithium. However, the lithium abundance corresponds to the Spite plateau lies significantly below the BBN predictions (A. Coc et al. 2004; R. H. Cyburt et al. 2016) by a factor of $2 \sim 3$ (L. Sbordone et al. 2010; P. Bonifacio et al. 2018). This discrepancy is referred as the "cosmological lithium problem." The physical reason for this discrepancy remains debated, with proposed solutions ranging from stellar lithium depletion to revisions of standard BBN. Early studies dismissed significant depletion due to the plateau's uniformity; however, lithium abundances inferred from CMB measurements now require astrophysical explanations, such as pre-main-sequence destruction (X. Fu et al. 2015) or inhomogeneous baryon density fluctuations (F. Iocco et al. 2009). Recent studies report $A(\mathrm{Li}) \sim 2.2$ in low-metallicity gas clouds, suggesting that stellar depletion may not fully resolve the cosmological lithium problem given that the Li abundance of the gas-phase cloud is not affected by this process (P. Molaro et al. 2024).

For stars with metallicity below ~ -2.5 dex, the constancy of the Spite plateau has been the subject of ongoing debate. Previous works have found that there is a "meltdown" or "break" of the Spite plateau. For example, S. G. Ryan et al. (1999) pointed out the slope and discussed the possible increase of lithium with metallicity even in the metal-poor range, assuming lower primordial abundance. P. Bonifacio & P. Molaro (1997) attributed the discrepancies to the biases in the temperature scale. L. Sbordone et al. (2010) showed that the scatter in lithium abundance increases as metallicity decreases for warm halo stars in the metallicity range between ~ -2.6 and ~ -3.5 dex. W. Aoki et al. (2009) reported that the average lithium abundances for stars with metallicity lower than -3.0 are lower by 0.2 dex than that of stars with higher metallicity. J. Meléndez et al. (2010) suggested two levels of the plateau for metallicity ranges higher and lower than [Fe/H] $= -2.5$. T. Matsuno et al. (2017) argued that stars might show some sort of plateau at [Fe/H] < -3.5. H. Li et al. (2022) found that the lithium plateau could be seen in turnoff stars, and the average Li abundance is clearly lower at lower metallicity. The meltdown of the Spite plateau may indicate a transition between primordial and stellar-produced lithium, but its exact cause remains debated.

In addition, recent works (e.g., A. Mucciarelli et al. 2012, 2022; H. Li et al. 2022) suggested that there is a thin lithium plateau in the metal-poor low red giant branch (RGB) stars, which indicate that the signal of a plateau can be preserved during stellar evolution, and thus, the signature (if there is any) of lithium abundance in evolved stars could be also used as constraints to the primordial value.

Non–local thermodynamic equilibrium (NLTE) effects critically influence abundance determinations, particularly for ionization-sensitive elements (e.g., G. Zhao et al. 1998; G. Zhao & T. Gehren 2000; T. Gehren et al. 2004; M. Asplund 2005; H. W. Zhang et al. 2006, 2008; J. R. Shi et al. 2008; S. A. Alexeeva et al. 2014; H. L. Yan et al. 2015; G. Zhao et al. 2016; L. Mashonkina et al. 2017b; S. Alexeeva et al. 2018, 2023). From another perspective, in studies of stars with metallicities as low as one-thousandth or even one-ten-thousandth of the solar value, LTE assumptions may underestimate effective temperatures (T_{eff}) by hundreds of Kelvins or overestimate [Fe/H] due to misinterpretations of Fe I/Fe II ionization balances (L. Mashonkina et al. 2017a). Previous works reported that the abundance discrepancy between Fe I and Fe II can be significant, reaching ∼0.4–0.8 dex under LTE assumptions (e.g., K. Lind et al. 2012; A. M. Amarsi et al. 2016; R. Ezzeddine et al. 2017; T. Nordlander et al. 2017). It should be noted that recent work reported consistent Fe I and Fe II abundances by an LTE analysis within uncertainties for HE 0107−5240 (E. Caffau et al. 2025), one of the most metal-poor stars (N. Christlieb et al. 2002), suggesting that the NLTE effects in the most metal-poor stars may require further investigation.

An NLTE analysis is crucially important for lithium studies as well. Recent studies have found that NLTE impacts line formation in 1D stellar atmosphere models when lithium abundance is extremely high (e.g., H. Li et al. 2018; H.-L. Yan et al. 2018). Meanwhile, combining NLTE with 3D models has refined the lithium abundance determinations for a massive amount of stars (E. X. Wang et al. 2021). Finally, T. Sitnova et al. (2015) and J. Shi et al. (2025, hereafter Paper I) revealed a systematic T_{eff} overestimation in LTE models, which may skew lithium abundance trends. By resolving such biases, an NLTE abundance analysis may help to clarify the "breakdown" of the Spite plateau at low metallicities and bridge observational data and theoretical models in the quest to resolve the lithium problem.

Given these facts, systematic NLTE analyses of both stellar parameters and elemental abundances of a large sample of metal-poor stars are of great importance. Such efforts have been done by a number of works. For example, T. Sitnova et al. (2015) and G. Zhao et al. (2016) presented systematic NLTE analyses to a large sample of metal-poor stars observed by the Lick telescope. Their program stars are down to the metallicity of ~ -2.4 dex. Later, W. Aoki et al. (2022), H. Li et al. (2022), and R. Zhang et al. (2024) carried out a more massive project that they studied over 400 very metal-poor (VMP) stars found by the LAMOST survey (X.-Q. Cui et al. 2012; G. Zhao et al. 2012; H. Yan et al. 2022) and observed by the Subaru telescope, but this work was done in the LTE assumption. A recent study by Paper I presented stellar parameters for over 100 VMP stars, taking advantage of NLTE line formation calculations for Fe I and Fe II. Paper I is the first paper in this series, which aims to present a systematic NLTE study of VMP stars with metallicity extended down to ~ -4.3 dex.

In this second paper, we present a homogeneous NLTE analysis of the lithium abundances for 103 VMP stars (with stellar parameters presented in Paper I). The paper is organized as follows: In Section 2, we present how our data are collected and selected; in Section 3; we present the method used for obtaining the stellar parameters, lithium abundance, NLTE corrections, and evolutionary stages for our sample stars; in Section 4, we present the lithium abundance result and how we

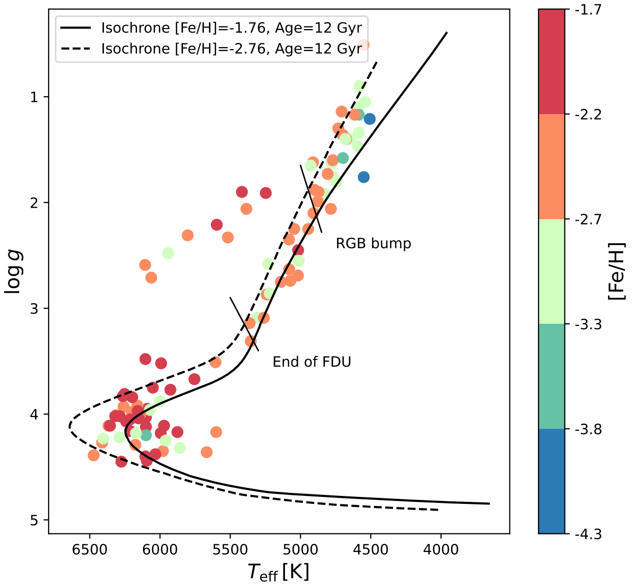

Figure 1. Distribution of our sample stars in the H-R diagram, color coded by [Fe/H]. The solid and dashed lines represent 12 Gyr Y^2 isochrones with $[Fe/H] = -1.76$ and -2.76, respectively. The approximate location of the first dredge-up (FDU) termination and the RGB-bump are indicated following the way of A. Mucciarelli et al. (2022).

come to our conclusions. Then, we show the summary in the final section Section 5.

2. Data

2.1. Observation and Sample Selection

We selected our program stars from a large sample that consists of ∼400 very metal-poor stars (W. Aoki et al. 2022; H. Li et al. 2022; R. Zhang et al. 2024), which were originally selected from the LAMOST survey and then observed by Subaru/High Dispersion Spectograph (HDS) during the years of 2014–2017 via a joint program. The observations were conducted with a resolution power of $R \sim 36{,}000$. Observation details can be found in W. Aoki et al. (2022).

For a reliable systematic NLTE analysis of VMP stars and a comprehensive investigation of the chemical evolution of the early Milky Way, we selected our program stars by the following criterion: (1) the signal-to-noise ratio (SNR) of their spectra are over 50 for stars with $[Fe/H] \geqslant -4.0$ at the range of 4500 Å; (2) they must cover the evolutionary stages from the unevolved main-sequence phase to the highly evolved phase of the horizontal branch (HB; see Paper I); (3) all stars with $[Fe/H] < -4.0$ are included regardless of their spectral SNR. This procedure yields a sample of 103 stars with metallicity down to −4.3 dex. We show our sample stars on an H-R diagram in Figure 1.

2.2. Stellar Parameters

Stellar atmospheric parameters were adopted from Paper I. These parameters were established with a two-step approach. The final uncertainties are typically 50–100 K in $T_{\rm eff}$, 0.2 dex in $\log g$, 0.1 dex in [Fe/H], and 0.2 km s^{-1} in ξ_t (see Paper I for details), providing a solid foundation for our subsequent elemental abundance determinations.

Table 1
Li Atomic Data

Wavelength	Transition	log *gf* (a, b)	log C_6 (c)
6707.76	$1s^22s - 1s^22p$	−0.002	−31.255
6707.91	$1s^22s - 1s^22p$	−0.299	−31.255
6103.54	$1s^23d - 1s^22p$	0.101	−30.317

Note.
References. (a) J. R. Shi et al. (2007), (b) H.-L. Yan et al. (2018), and (c) P. S. Barklem et al. (1998).

3. Methods

3.1. Measurement of Li Abundance

We use the spectrum synthesis method to derive the lithium abundances. A spectral synthesis analysis used an IDL-based software package *SIU* (J. Reetz 1999) and grids of MARCS atmospheric models (B. Gustafsson et al. 2008). For most of our program stars, lithium abundances were measured using the resonance Li I doublet at 6707.76 and 6707.91 Å. For the four Li-rich stars in our sample, the subordinate line at 6103.6 Å is strong enough to derive reliable lithium abundances. In these four stars, both the resonance line and subordinate line were used. The data of the atomic line are listed in Table 1.

The lithium abundance is expressed as A(Li): $A(Li) = \log(N_{\rm Li}/N_{\rm H}) + 12$, where $N_{\rm Li}$ and $N_{\rm H}$ represent the number densities of lithium and hydrogen in stars, respectively. To fit the observed spectral line profiles, spectral broadening caused by rotation, macroscopic turbulence, and instrumental broadening have been taken into account as a Gaussian broadening profile.

3.2. NLTE Calculation

NLTE effects were taken into account in our determination of lithium abundances. We used the lithium atomic model developed by J. R. Shi et al. (2007). To solve the coupled radiative transfer and statistical equilibrium equations, we employ a revised version of the *DETAIL* program based on the accelerated lambda iteration method (G. B. Rybicki & D. G. Hummer 1991, 1992), as updated by L. Mashonkina et al. (2011). The resulting departure coefficients were then utilized by *SIU* to compute NLTE synthetic line profiles. In Figure 2, we present several examples of the line profile fitting results at the resonance Li I lines of both LTE and NLTE analyses. The NLTE effects for Li abundance are defined and calculated by $A(Li)_{\rm NLTE} - A(Li)_{\rm LTE}$. It is important to note that, in stars with extremely high lithium abundances, the Li I lines are strong, and the LTE-based line profile fitting fails to reproduce the observed profiles, whereas NLTE calculations provide a much better match.

3.3. Determination of Evolution Phase

To assess the evolutionary phase of our sample stars, we compare their observed effective temperatures and surface gravities with theoretical isochrones computed at an age of 12 Gyr. The isochrone models adopted in this work are drawn from the grid presented by S. K. Yi et al. (2004), which assumes a fixed [α/Fe] enhancement of 0.4 dex. However, because the available isochrone models are produced only at a

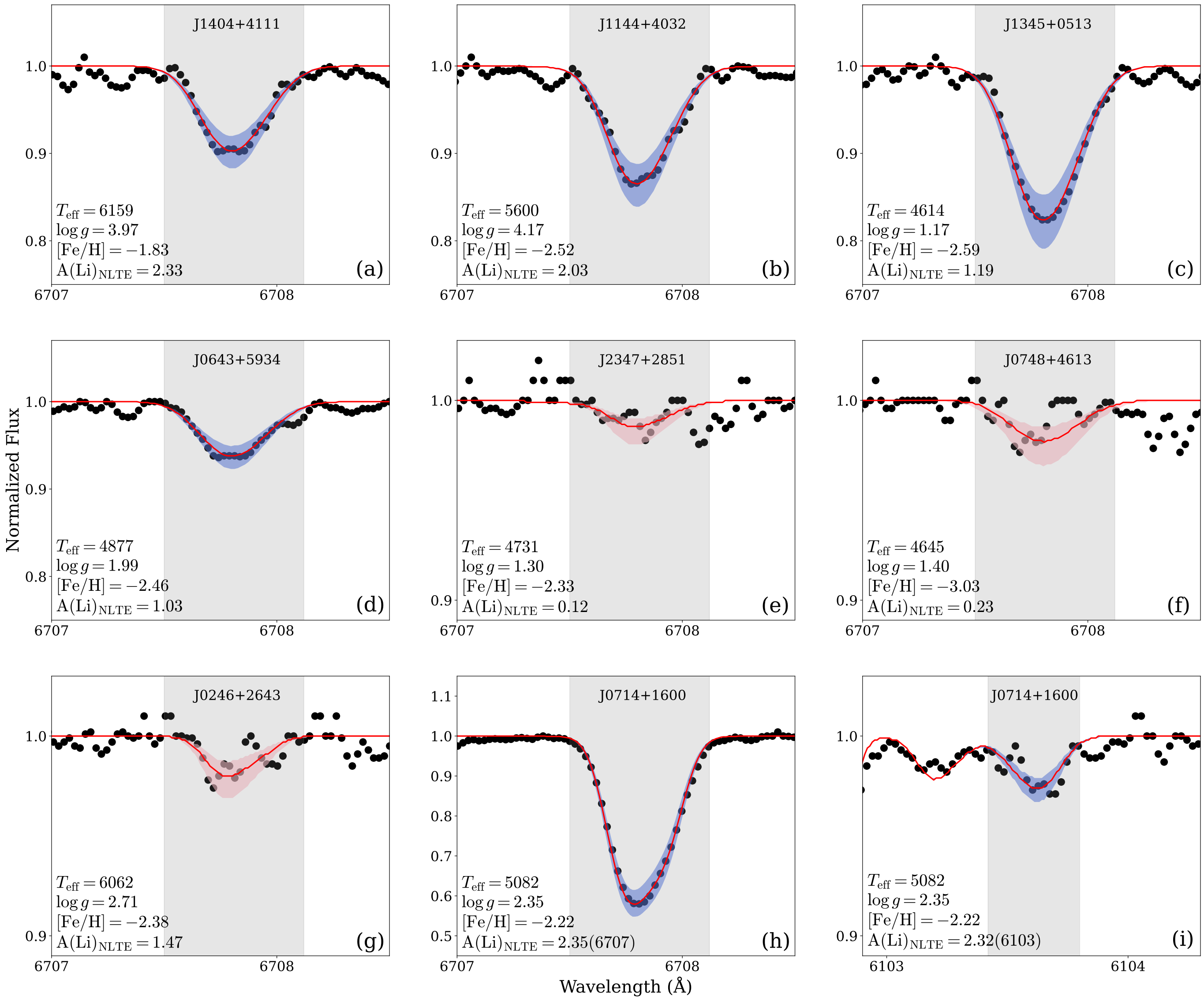

Figure 2. The examples of line profile fittings in this work. In all the panels, the black dots are the observed spectra, and the red lines are the theoretical spectra. Panels (a) and (b) show two fitting examples of unevolved stars. Panels (c) and (d) show two fitting examples of LRGB stars. Panels (e) and (f) show "upper limit" fittings of two highly evolved RGB stars, and panel (g) shows an "upper limit" fitting to a high temperature HB star. Panels (h) and (i) show fittings to the resonance line and subordinate line of a Li-rich star, respectively. The blue areas represent synthesis spectra with $A(\rm Li)_{\rm NLTE} \pm 0.1$ dex in panels (a), (b), (c), (d), (h), and (i), while the red areas represent synthesis spectra with $A(\rm Li)_{\rm NLTE} \pm 0.2$ dex in panels (e), (f), and (g).

few discrete metallicities, an isochrone corresponding to a specific iron abundance cannot be obtained directly.

To overcome this, we generate the desired 12 Gyr isochrone by linearly interpolating between the two bracketing models. In our approach, the measured [Fe/H] is first converted to a corresponding metallicity; then, when the target metallicity does not exactly match one of the discrete model values, an interpolation is performed between the model that is just higher and that just lower than the target. This procedure yields a synthetic isochrone that reflects the target metal content.

We apply this interpolation method to our sample, which is divided into four [Fe/H] bins. These bins are defined as follows: stars with $[\rm Fe/H] > -2.5$, stars with [Fe/H] between -2.5 and -3.0, stars with [Fe/H] between -3.0 and -3.5, and stars with $[\rm Fe/H] < -3.5$. For each bin, a representative [Fe/H] value is adopted (namely, 2.25, 2.75, 3.25, and 3.75, respectively) to perform the interpolation.

4. Results and Discussion

4.1. Lithium Abundance and Uncertainty Estimation

We obtained the LTE and NLTE lithium abundances for 77 stars in our sample. For 23 of the remaining stars, their lithium lines are not very clear but marginally recognizable, we performed a fitting using slightly stronger line profiles and adopted the derived abundances as upper limits for A(Li), and most of these stars are highly evolved stars. For the last three stars, we cannot detect any lithium features in their spectra, and we do not present a lithium abundance or upper limit for these three stars. The results of the Li abundance obtained from both LTE and NLTE analyses are listed in Table 2 (and Table A1 in the Appendix) together with the stellar parameters. Most of the lithium abundance and all the upper limits shown in Tables 2 and A1 are derived from the resonance Li I line, as we previously mentioned, while, for the

Table 2
Li Abundance and Stellar Parameters

Star	$T_{\rm eff}$ (K)	log g (dex)	[Fe/H]	ξ_t (km s^{-1})	A(Li)$_{\rm LTE}$	A(Li)$_{\rm NLTE}$	Phase
J0055 + 1857	5018	2.69	−2.26	1.40	0.94	0.97	2
J0119 + 2425	6412	4.27	−2.57	1.64	2.18	2.17	1
J0131 + 4800	6100	4.03	−1.79	1.35	2.21	2.23	1
J0232 + 0545	6091	3.95	−2.16	1.11	2.34	2.35	1
J0244 + 0828	6472	4.39	−2.27	1.60	2.48	2.47	1
J0246 + 2643	6062	2.71	−2.38	3.30	1.44	1.47	4
J0326 + 0202	4827	1.92	−3.05	1.52	0.85	0.88	3
J0352 + 0514	5859	4.32	−3.11	1.20	1.99	1.99	1
J0423 + 0538	6100	4.12	−2.04	1.31	2.33	2.34	1

Note. Phases: (1) unevolved stars, (2) RGB stars, (3) highly evolved RGB stars, and (4) horizontal branch.

four Li-rich stars, their abundances are an averaged value of the resonance Li I line and the subordinate line. The differences between these two lines are from 0.03 to 0.20 dex with an average of 0.12 dex for these four stars.

Our sample overlaps with that of H. Li et al. (2022), which presented the lithium abundance in LTE. In Figure 3, we show a comparison of the LTE lithium abundances with the previous work. Li-rich stars are not included in this comparison, as the LTE abundances in super-Li-rich stars are not reliable. For most stars, they show a strong connection with the difference in effective temperatures, which is expected since the abundance of lithium is sensitive to $T_{\rm eff}$. The mean difference is 0.05 dex with a scatter of 0.12 dex.

In Figure 4, we show the NLTE Li abundance as a function of the effective temperature of our program stars. Given the wide range of metallicity in our sample stars, the overall trend is consistent with our previous work (G. Zhao et al. 2016) and many other works (e.g., A. Bandyopadhyay et al. 2022). Four outliers show an anomaly of high Li abundance compared with other stars at their evolutionary stages, which are identified as Li-rich stars (detailed discussions are presented in Section 4.4). Except for the Li-rich stars, all the other stars show a Li abundance that is significantly lower than the predicted value from BBN. The Spite plateau can be clearly seen from Figure 4, panel (b), and we present these details in Section 4.3.

In Figure 5, we show the NLTE effects of the Li resonance lines at 6708 Å in our sample stars as functions of $T_{\rm eff}$, log g, [Fe/H], and A(Li)$_{\rm LTE}$. For most of our program stars, the NLTE effects are not very large, and the absolute values of the difference are at a level of ∼0.05 dex. For the four Li-rich stars, this effect can reach ∼0.60 dex, which is consistent with what is reported by previous work (e.g., H.-L. Yan et al. 2021). To avoid clutter and to provide a clearer view of the majority of the stars, the NLTE effects of the three most Li-rich stars are not shown in Figure 5 but presented in the caption of the figure.

The uncertainty of the Li abundance was mainly caused by the uncertainties of stellar parameters (namely, $T_{\rm eff}$, log g, [Fe/H], and ξ_t). Thus, we tested three stars from the VMP sample by varying the stellar parameters within their typical uncertainties, which are $\Delta T_{\rm eff} = \pm 100$ K, $\Delta \log g = \pm 0.10$ dex, and Δ[Fe/H] $= \pm 0.10$ dex, $\Delta \xi_t = \pm 0.2$ km s^{-1}, respectively. The results are shown in Table 3. The Li abundance is more sensitive to the $T_{\rm eff}$ than that of other stellar parameters. Our final uncertainty of the lithium abundance is estimated from the weighted average of the errors due to the uncertainties in the three parameters.

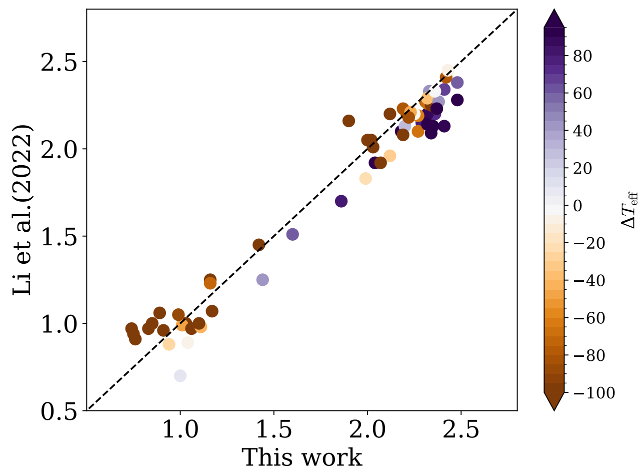

Figure 3. Comparison of the LTE Li abundances with our previous work (H. Li et al. 2022). The difference in effective temperatures (this work − literature) is indicated with a color bar on the right. Li-rich stars are not included in this comparison, as the LTE abundances in super-Li-rich stars are not reliable.

4.2. Evolutionary Phases

Figure 6 presents the isochrones of our program stars and their lithium abundances in a 2 × 2 layout. In each panel, the dashed line shows the interpolated 12 Gyr isochrone appropriate for the designated [Fe/H] bin, while the filled black circles denote the observed stellar parameters. The effective temperature and surface gravity axes are inverted following standard astronomical conventions. The overall agreement between the observed positions and the interpolated isochrones confirms the robustness of our spectroscopic measurements and provides a reliable means to determine the evolutionary phases of stars over a wide metallicity range. For a better classification, we also marked the rough positions of the end of the first dredge-up (FDU) and RGB-bump in each panel, respectively (A. Mucciarelli et al. 2022). Based on the positions of our program stars, they are classified as four groups: the unevolved stars (stars that have not reached FDU), lower RGB (LRGB) stars (stars between FDU and RGB-bump), highly evolved stars (stars that passed the RGB-bump), and the HB stars (stars to the left of the dashed isochrone lines).

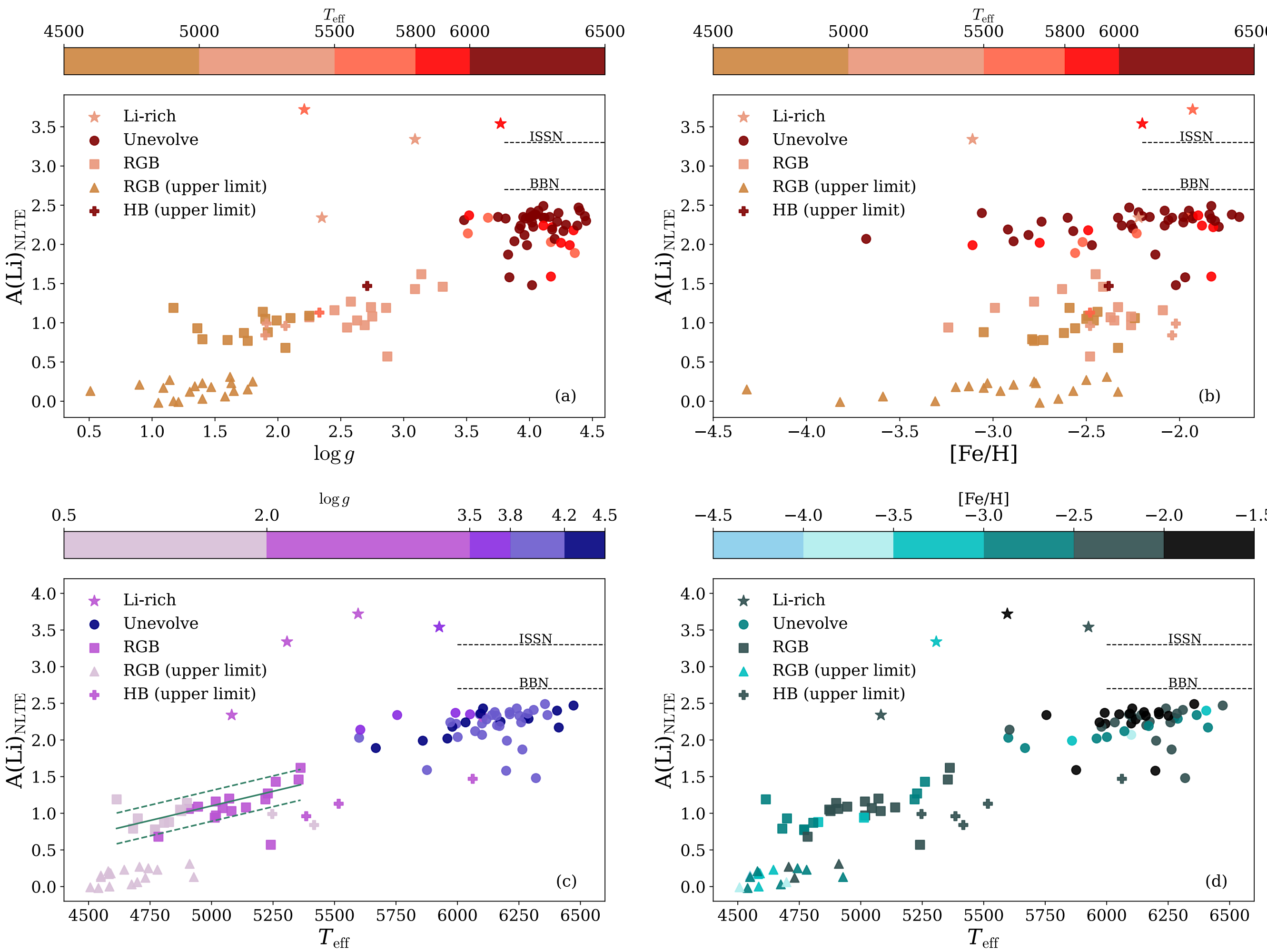

Figure 4. The NLTE Li abundances as functions of stellar parameters. Panels (a) and (b) show the NLTE Li abundance as functions of surface gravity and metallicity, with effective temperature as a color bar. Panels (c) and (d) show the NLTE Li abundance as a function of effective temperature, with surface gravity and metallicity as color bars, respectively. The horizontal dashed lines with BBN represent the Li abundance predicted by the standard BBN theory, while the other horizontal dashed lines with ISSN represent the Li abundance of the initial solar system nebula. The four Li-rich stars are indicated as pentagons. The carbon-enhanced metal-poor (CEMP) stars are indicated with a gray circle surrounding specific symbols. The lithium gap can be seen in panel (a) of this figure.

4.3. The Lithium Plateaus and the Lithium Gap

4.3.1. The Spite Plateau and Its Meltdown in Unevolved Stars

The lithium abundance in warm, metal-poor Population II stars is commonly regarded as a proxy for the primordial value (M. Spite & F. Spite 1982b). For our data as seen in Figure 4, the unevolved warm metal-poor halo stars with an effective temperature between 6500 and 6000 K and [Fe/H] between −2.5 and −1.7 dex show a Li plateau (Spite plateau) at A(Li) =2.32 dex (hereafter referred to as plateau stars). This value is consistent with many previous studies (e.g., R. Rebolo et al. 1987; P. Bonifacio & P. Molaro 1997; C. M. Gutiérrez et al. 1999; S. G. Ryan et al. 2000; H.-W. Zhang & G. Zhao 2003; J. Meléndez & I. Ramírez 2004; P. Bonifacio et al. 2007, 2018; J. R. Shi et al. 2007; W. Aoki et al. 2009; A. Hosford et al. 2009; L. Monaco et al. 2010; L. Sbordone et al. 2010; M. Schaeuble & J. R. King 2012; G. Zhao et al. 2016; P. Molaro et al. 2020; C. L. Kielty et al. 2021).

However, there is an argument about if the Spite plateau is strictly flat. For a better investigation of the Spite plateau, in addition to Figure 4, we show the Li abundances (including ours and those in the literature) as functions of [Fe/H] and the linear fitting to the trend in Figure 7. In the upper panel of Figure 7, we present a linear fit to the unevolved plateau stars ($\log g \geqslant 4.0$). The best linear fit is $A(Li) = (0.17 \pm 0.07) \times [Fe/H] + 2.67$. The standard deviation of the lithium abundances in these unevolved plateau stars is 0.10 dex. Under both LTE and NLTE assumptions, the trends of A(Li) with [Fe/H] remain the same, with only minor differences in the fitted slopes given that NLTE corrections for our sample stars as a function of [Fe/H] show no obvious trend as seen in Figure 5. Similarly, 3D effects are not expected to introduce a strong systematic trend with metallicity.

It has been reported that the Spite plateau breaks for stars with metallicity lower than ∼−2.5 dex (e.g., W. Aoki et al. 2009; L. Sbordone et al. 2010). The deviations from the Spite plateau can be interpreted as hints at mechanisms of lithium depletion acting during the lifetime of Population II stars (E. Martín 2023). In our program stars, there is indeed a decline and larger scatter of the lithium abundance toward the metal-poor end; however, as seen from the upper panel of Figure 7, the lithium abundance in stars with effective temperatures higher than 6000 K (warm) remains in a thin plateau with very narrow variations. For our warm unevolved

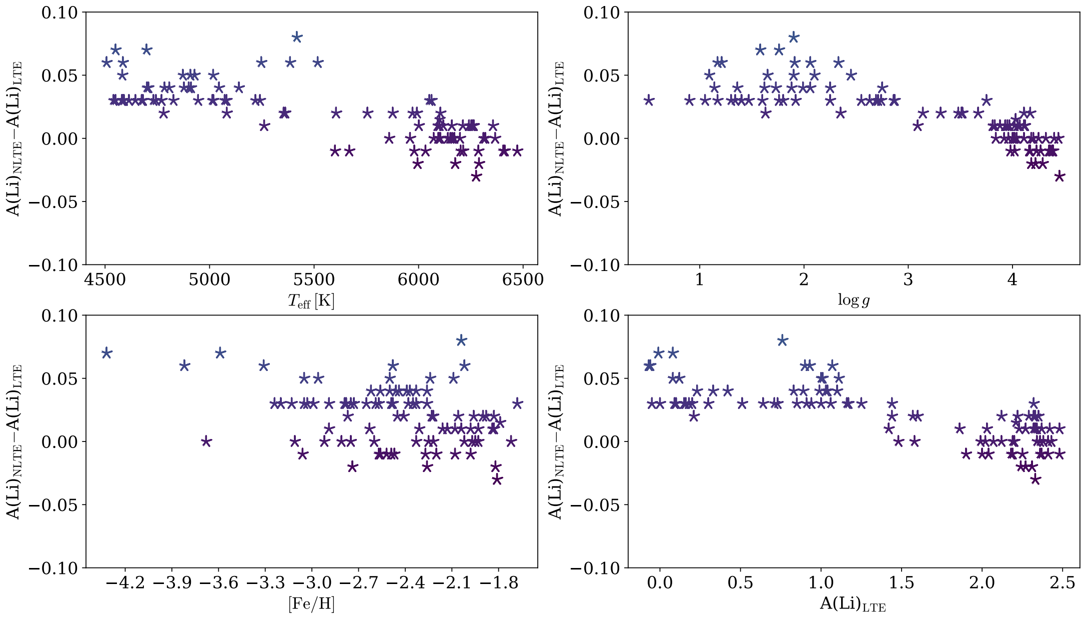

Figure 5. $A(Li)_{NLTE} - A(Li)_{LTE}$ of our work versus stellar parameters and $A(Li)_{LTE}$. The result of $A(Li)_{NLTE} - A(Li)_{LTE}$ for the three most Li-rich stars: J0554 + 5235, J0626 + 6032, and J0705 + 2552 are −0.32, −0.18, −0.60 dex, respectively. These Li-rich stars are not shown in Figure 5 to avoid clutter and to provide a clearer view of the corrections for the majority of the stars.

Table 3
Li Abundance Errors Due to the Uncertainties in the Stellar Parameters

	Input Error	J2217	J1404	J0554
	T_{eff} (K)	4507	6159	5596
ΔA(Li)	+100	+0.11	+0.07	+0.10
	−100	−0.08	−0.07	−0.10
	logg (dex)	1.21	3.97	2.21
ΔA(Li)	+0.10	+0.01	0.00	0.00
	−0.10	−0.01	0.00	0.00
	[Fe/H] (dex)	−3.82	−1.83	−1.93
ΔA(Li)	+0.10	0.00	0.00	−0.01
	−0.10	0.00	0.00	+0.01
	ξ_t (km s^{-1})	2.40	1.35	2.30
ΔA(Li)	+0.20	+0.01	0.00	0.00
	−0.20	0.00	0.00	0.00

sample stars, there is a small gap in metallicity of ∼−2.6. Thus, we perform two linear fittings to warm stars with a metallicity higher and lower than −2.6 dex, respectively. Interestingly, they show a very similar slope (0.17 versus 0.11) and A(Li) scatter (0.10 dex versus 0.13 dex), respectively (see the blue and green lines in the upper panel of Figure 7). To rule out the sample effect, we extended the sample by including more stars from the literature (P. Bonifacio et al. 2007; W. Aoki et al. 2009; L. Sbordone et al. 2010; G. Zhao et al. 2016; T. Matsuno et al. 2017), and performed the same fitting procedure, as shown in the lower panel of Figure 7. We found a similar result: the classic Spite plateau shows a slope of 0.20 with a A(Li) scatter of 0.10 dex, and the "meltdown" stars show a slope of 0.14 with a A(Li) scatter of 0.10 dex. Given this result, one can estimate that the average lithium abundances at [Fe/H] = −3.0 *and* = −3.5 will be lower than those at [Fe/H] = −2.0 by ∼0.17 dex and ∼0.24 dex, which is consistent with the value reported in previous work (e.g., S. G. Ryan et al. 1999; W. Aoki et al. 2009; T. Matsuno et al. 2017).

The overall trend of the metallicity-extended Spite plateau decreases toward the metal-poor direction. This result suggests that the classic Spite plateau is not strictly flat; most significantly, it is likely to extend to lower metallicities as some previous work suggested (e.g., T. Matsuno et al. 2017). However, the behavior of lithium abundances below [Fe/H] < −3.0 remains debated. The so-called "meltdown" of the Spite plateau has been interpreted either as an increased scatter in lithium abundances or as a systematic decline toward lower metallicity. It should be mentioned that, in our sample, only one unevolved star reaches [Fe/H] ∼ −3.6, which prevents a firm conclusion regarding the presence or absence of increased scatter in this region. Recent studies of extremely metal-poor (EMP) stars (e.g., D. S. Aguado et al. 2019; A. M. Matas Pinto et al. 2021) have reported diverse lithium behaviors at the lowest metallicities. Further investigations with larger samples are required to clarify whether a true breakdown of the plateau occurs.

The slightly positive slope of the extended Spite plateau may indicate that, in addition to the primordial component, a small amount of Galactic lithium production has already taken place at early times. Nova has been suggested to be one of the main contributors to the Galactic lithium enrichment (e.g., M. Arnould & H. Norgaard 1975; S. Starrfield et al. 1978, 2024; M. Hernanz et al. 1996; J. José & M. Hernanz 1998; P. A. Denissenkov et al. 2014; L. Izzo et al. 2015; A. Tajitsu et al. 2015; P. Molaro et al. 2016; P. Selvelli et al. 2018; A. Arai et al. 2021; A. J. Kemp et al. 2022; P. Molaro et al. 2022; J. Gao et al. 2024; T. Matsuno et al. 2025). While nova enrichment is expected to become important at higher metallicities (D. Romano et al. 2021; S. Borisov et al. 2024), current models remain relatively unconstrained in the metal-poor regime. Given the substantial lithium yield of individual events, early novae could still provide a nonnegligible contribution to lithium enhancement in VMP stars considered in this work. Additionally, cosmic-ray spallation operates from early epochs and behaves predominantly as a metallicity-

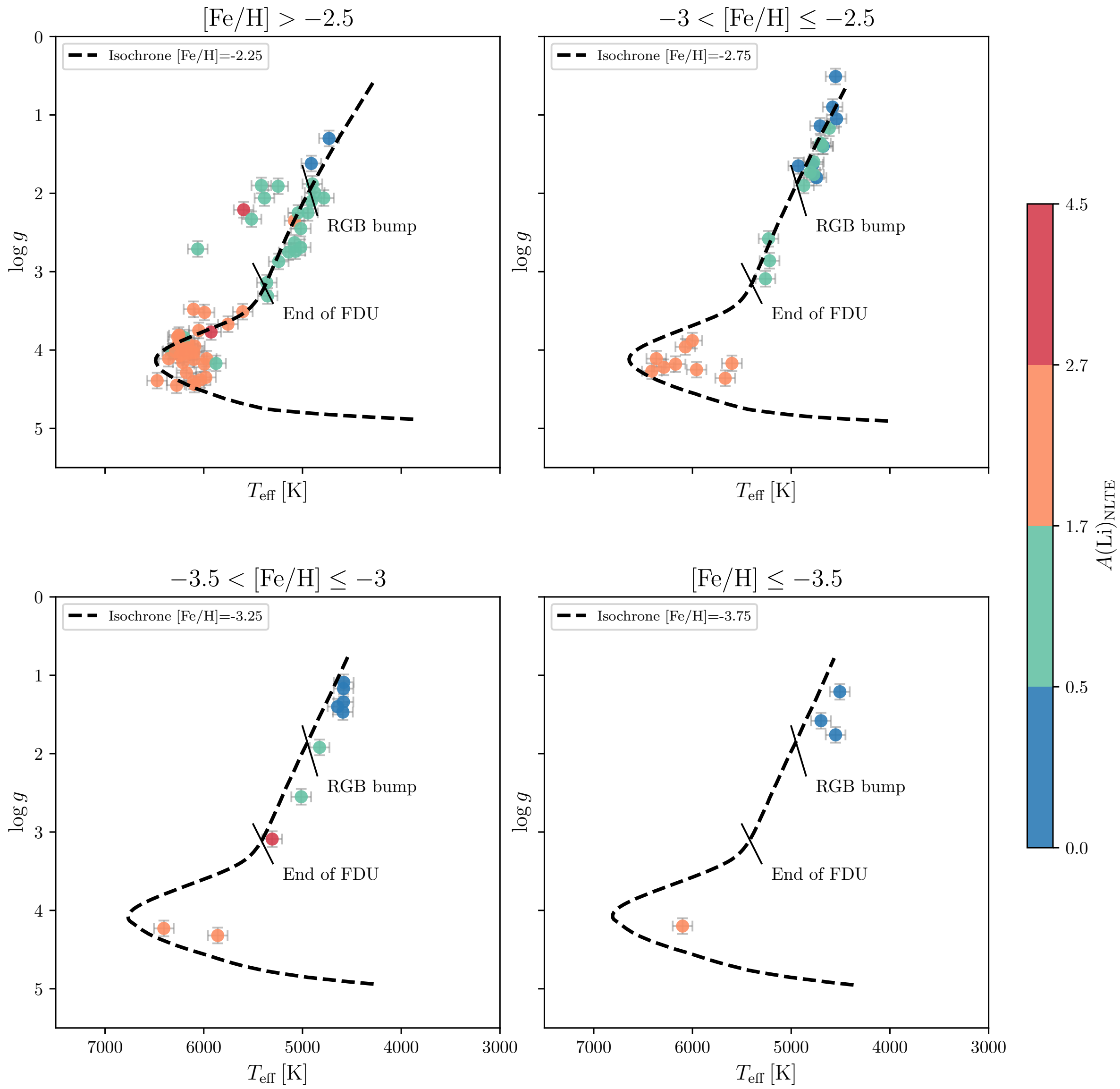

Figure 6. 12 Gyr Y^2 isochrones for stars grouped by metallicity, shown in four panels with different [Fe/H] intervals: [Fe/H] > -2.5 (isochrone interpolated at [Fe/H] $= -2.25$), $-2.5 \geqslant$ [Fe/H] > -3.0 (isochrone at -2.75), $-3.0 \geqslant$ [Fe/H] > -3.5 (isochrone at -3.25), and [Fe/H] < -3.5 (isochrone at -3.75). Dashed lines represent the interpolated theoretical isochrones, and filled colored circles denote the observed stellar parameters, with the color bar indicating $A(\mathrm{Li})_{\mathrm{NLTE}}$. As in Figure 1, each panel marks the approximate positions of the RGB-bump and the end of FDU.

dependent process (e.g., M. Lemoine et al. 1998; V. Grisoni et al. 2019). While such behavior is qualitatively consistent with an increase of the lithium abundance with increasing [Fe/H], chemical evolution models (e.g., N. Prantzos 2012) suggest that its contribution at very low metallicity is limited, and may not be sufficient alone to account for the observed trend in our sample. A joint contribution from both early Galactic enrichment mechanisms may be required.

Meanwhile, we note that such a slope could also be interpreted as a signature of metallicity-dependent stellar depletion. While the Spite plateau is generally considered to be depleted from the primordial value (A(Li) $\simeq$ 2.7) due to the processes such as diffusion and macroturbulence (e.g., see C. Charbonnel & N. Prantzos 2026, for a recent review), a scenario that the depletion efficiency decreases with increasing metallicity could also naturally reproduce this positive slope.

The observed lithium trends in VMP stars likely result from a complex interplay between these internal stellar processes and early Galactic enrichment. Further observational constraints and detailed chemical evolution modeling will be essential to clarify the origin of this trend

4.3.2. The "Plateau" in Lower RGB Stars

With stars evolving to the RGB phase, the Li abundance in our sample exhibits additional features. The apparent dependence on surface gravity seen in Figure 4 largely reflects the underlying correlation with effective temperature, which is the dominant parameter in this region. More than half of the RGB stars in our sample have surface gravities between ∼2.0 and ∼3.0 dex and effective temperatures from ∼4800 to ∼5400 K. In Figure 6, we identify these stars lying between the end of FDU and RGB-bump, which is classified as LRGB. Previous work has reported the clue or evidence for the existence of a LRGB Li plateau. For example, K. Lind et al. (2009) showed that the Li abundances of LRGB stars in the metal-poor globular cluster NGC 6397 are around 1.10 dex.

A. Mucciarelli et al. (2012, 2022) found a thin plateau among LRGB stars with an average A(Li) = 1.09 ± 0.01 dex and a dispersion of $\sigma = 0.07$ dex. These LRGB stars span a relatively narrow effective temperature range of ∼5000–5350 K and a large range of metallicity from from −1.7 down to −7.0 dex. They also identified a small fraction of such stars with A(Li) < 0.7 dex. H. Li et al. (2022) reported that the Li abundance of giants remains more or less constant after the FDU to the RGB-bump.

In our program stars, we found a similar plateau in LRGB stars. Considering A. Mucciarelli et al. (2022)'s effective temperature range of 4800 to 5300 K as they show in their Figure 2, the stars in our sample (marked with a thick purple open square in Figure 7, top panel) show a mean lithium abundance of 1.13 ± 0.13 dex, with almost a zero slope in A(Li)–[Fe/H] plane. Additionally, a fitting to the lithium abundance as a function of effective temperature shows a nonzero slope, which is 0.12 ± 0.03, slightly larger than that reported by A. Mucciarelli et al. (2022). Extending the fitting range to a larger effective temperature range (e.g., from 4800 to 5400 K for LRGB stars) results in a very similar result.

It is noteworthy that the positive lithium-metallicity slope observed in unevolved stars is not preserved in the LRGB phase. This can be understood as a consequence of lithium depletion during the FDU process. Stellar evolution models (e.g., C. P. Deliyannis et al. 1990; I.-J. Sackmann & A. I. Boothroyd 1999; A. Mucciarelli et al. 2012) indicate that the FDU dilution is metallicity dependent, which tends to smooth out the initial slope. Thus, the depletion during stellar evolution may lead to the constant LRGB plateau universally observed, consistent with the findings of A. Mucciarelli et al. (2022) and this work.

4.3.3. The Lithium Evolution from LRGB to Highly Evolved RGB

As a star evolves from the LRGB to a higher stage, lithium becomes more depleted, and its abundance becomes difficult to measure. In our sample, 29 stars have been identified as highly evolved RGB stars, and 18 of them do not have detectable lithium. In such a situation, we provide only the upper limits for these stars. From Figures 4 and 7, there is a clear drop in abundance from A(Li) ∼1.0 to A(Li) < 0.5 dex although most lithium abundances in highly evolved RGBs are adopted as upper limits. A similar rapid depletion has been reported in globular clusters. K. Lind et al. (2009) demonstrated that lithium depletes abruptly at $M_v \sim 3.3$ in NGC 6397, which corresponds to the luminosity of LRGB in this globular cluster. Although the situation in field stars is more complicated, our sample stars exhibit a comparable rapid Li depletion. This behavior is consistent with the framework of noncanonical extra mixing. It is often triggered near the luminosity-function bump and may be driven by magnetically enhanced thermohaline mixing, rotation-induced meridional circulation, or internal gravity waves (R. Guandalini et al. 2009; S. Palmerini et al. 2011; N. Lagarde et al. 2019).

In addition, while the abundances for highly evolved stars are close to the detection limits and thus are only available as upper limits, these upper limits tend to cluster at similarly low abundance levels, as shown in Figure 7. This may reflect the natural evolutionary continuation of lithium depletion from the Spite plateau through the LRGB phase and into the highly evolved RGB stage under sustained, extra mixing. Although the current data are limited by detection thresholds, this pattern may provide a useful reference for future studies of lithium evolution in EMP highly evolved stars.

It is worth noting that we cannot rule out the possibility that these highly evolved stars are, or at least part of them are, asymptotic giant branch (AGB) stars. Their classification may influence the discussion of Section 4.3.4.

4.3.4. Li Abundance in Horizontal Branch Stars

The HB stars in our sample can be seen in the top left panel of Figure 6. These stars are marked with a thick cross in Figures 4 and 7. Due to their higher effective temperatures, HB stars exhibit lithium lines that are similarly weak as those in highly evolved RGB stars; thus, we also take the lithium abundances in HB stars as upper limits except for one super-Li-rich HB star. As shown in Figure 7, the upper limits for HB stars are systematically higher than the values of highly evolved RGB stars by approximately 1.0 dex. However, this comparison involves two sets of upper limits and should therefore be interpreted with caution. To confirm this apparent difference, further studies for HB stars with better signal-to-noise spectra are desirable.

4.4. Li-rich VMP Stars

The anomalous lithium enhancement in low-mass metal-poor stars has been investigated by previous work (e.g., H. Li et al. 2018; T. Matsuno et al. 2025). These Li-rich stars are distributed across a relatively wide range of evolutionary stages, from main-sequence stars to red giant branch stars, but their anomalous surface A(Li) cannot be explained by current stellar evolution models.

In our investigated sample, four common Li-rich stars are identified. These four stars are at different evolutionary stages: one is a turnoff star (J0626+6032), two are RGB stars (J0705+2552 and J0714+1600), and one is an HB star (J0554+5235). These stars exhibit varying degrees of lithium enhancement. Specifically, the NLTE A(Li) of the RGB J0714+1600 is 2.34 dex, while that of the other three stars exceeds the lithium abundance of the initial solar system nebula (ISSN). J0554 = 3.72 J0626 = 3.54 J0705 = 3.34

Figure 8 presents their abundance patterns, with results derived from the NLTE analysis in follow-up articles in this series. For the turnoff star J0626+6032 with A(Li) = 3.54, its Na abundance shows a slight enhancement but remains within the normal range, while the abundance of other elements of this star does not show any enhancement. For the HB star J0554+5235 with A(Li) = 3.72, it shows a normal slight Mg enhancement but also exhibits a Eu enhancement. The abundance patterns of the two stars are completely different. For the LRGB star J0714+1600 with A(Li) = 2.34, it only shows a small amount of Mg enhancement, while, for the other LRGB star J0705+2552 with A(Li) = 3.34, it shows strong C, Mg, and Ba enhancements. J0705+2552 has been identified as a carbon-enhanced metal-poor (CEMP) star. All of these stars show different abundance patterns compared to the one reported by T. Matsuno et al. (2025).

The mechanism for lithium enhancement is complex and is not yet fully understood. Hypernovae are considered as a potential source to produce lithium, as their high-energy environments can induce spallation reactions of CNO nuclei (B. D. Fields et al. 2002; K. Nakamura & T. Shigeyama 2004). L. Monaco et al. (2025) found the metal-poor star BPM 3066

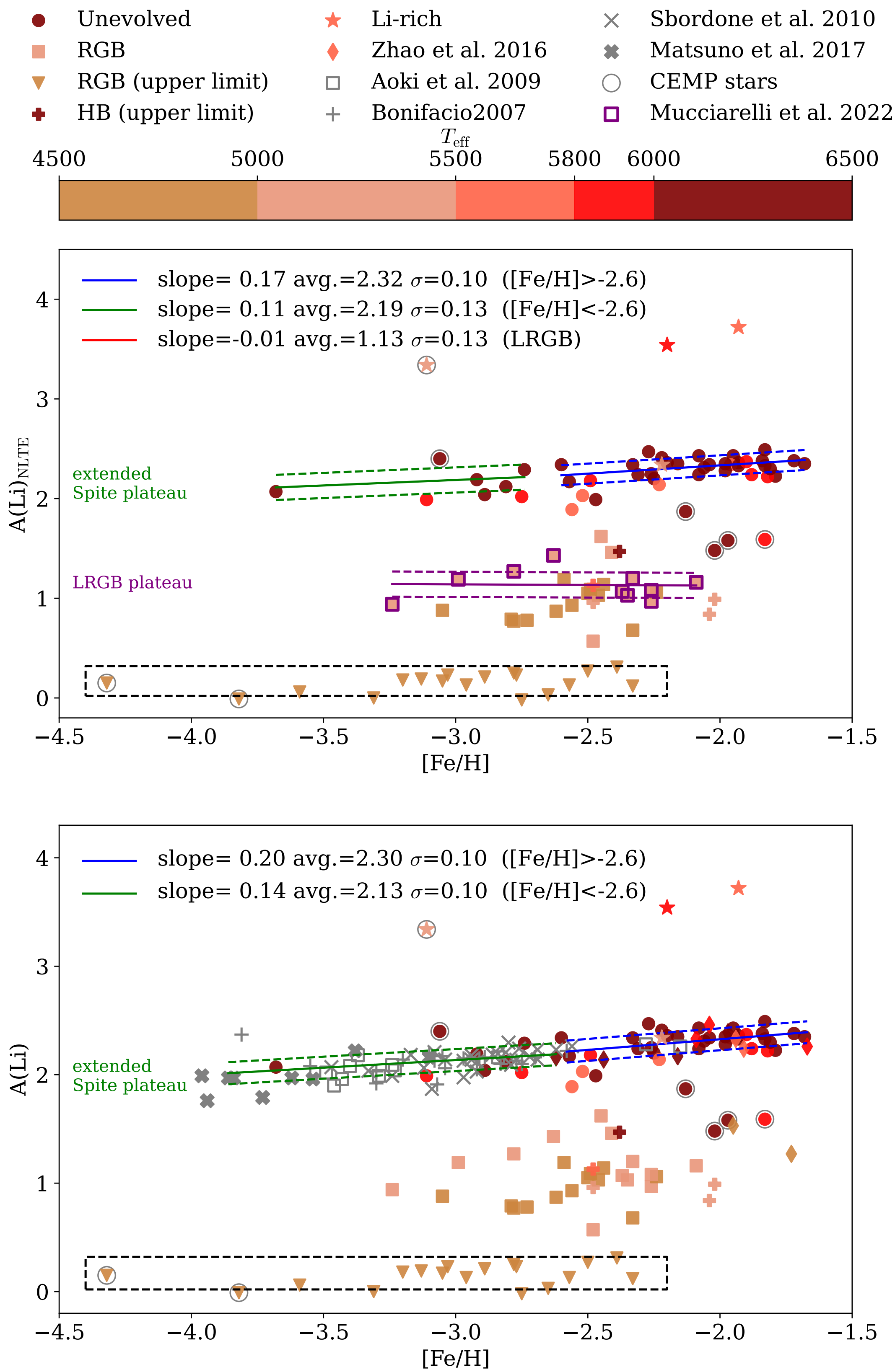

Figure 7. The NLTE lithium abundance and fittings to lithium plateaus. The upper panel shows stars in our sample, while the lower panel shows stars in our sample and from literature (P. Bonifacio et al. 2007; W. Aoki et al. 2009; L. Sbordone et al. 2010; G. Zhao et al. 2016; T. Matsuno et al. 2017). Symbols are the same with Figure 4. Squares outlined in thick purple indicate the subsample selected following A. Mucciarelli et al. (2022). CEMP stars are indicated with a gray circle surrounding the specific symbols. The lithium gap can be seen in all panels of this figure and panel (a) of Figure 4.

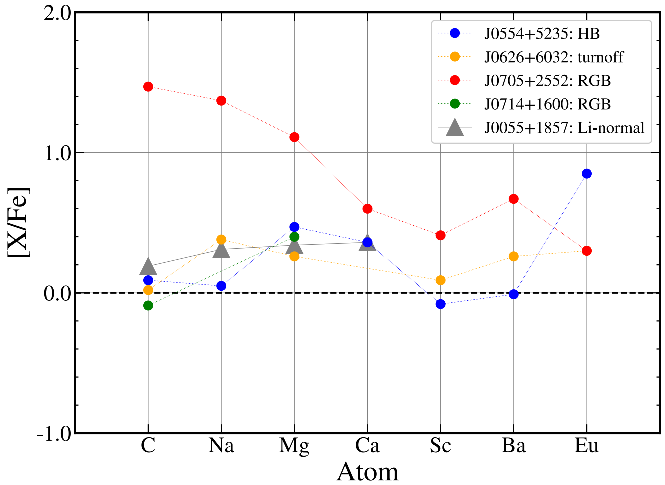

Figure 8. The elemental abundances of four Li-rich stars in our sample and one Li-normal star with a similar [Fe/H] in our sample as a comparison. The abundances are presented using NLTE results. For [Eu/Fe] of J0626+6032 and J0705+2552, a limiting value of 0.3 dex is applied. The solar abundances are adopted from M. Asplund et al. (2021).

to be strongly enriched in both Li and Be, with a $^{7}Li/^{9}Be$ ratio of 7.9 matching spallation yields. However, coenhancements of Li and Na may contradict hypernova predictions. In our Li-rich sample, J0626+6032 shows a moderate Na enhancement. While J0705+2552 has exceptionally high Li and Na enrichment (also see H. Li et al. 2018), two other VMP stars have been reported to show similar Li and Na enrichment (I. U. Roederer et al. 2014; A. Mucciarelli et al. 2024).

Another possible mechanism that has been proposed to explain lithium enhancement is the engulfment of planetary material or a brown dwarf companion (J. B. Alexander 1967; J. F. Ashwell et al. 2005). Though, the engulfment mechanism faces two challenges in fully explaining the high Li abundances observed in these stars. First, the maximum A(Li) after ingestion is usually below 2.2 dex for giants (C. Aguilera-Gómez et al. 2016). Second, the occurrence rate of planets around metal-poor stars has been debated, with early studies suggesting that this rate is low (A. Koch et al. 2011; L. Ghezzi et al. 2018), which would reduce the likelihood that all four Li-rich stars would experience engulfment events. However, as demonstrated by L. Monaco et al. (2025), the planetary number may be substantial for stars with [Fe/H] < -1 dex, and observations have confirmed planets around stars with metallicities as low as [Fe/H] ~ -2 dex (L.-J. Li & S.-B. Qian 2014). Three stars (J0554+5235, J0626+6032, J0714+1600) in our Li-rich sample have metallicities similar to that of the confirmed planet-hosting star. While J0705+2552 has [Fe/H] below ~ -3 dex, where planet occurrence remains uncertain, engulfment remains plausible but unconfirmed for this star.

Among the four Li-rich stars, J0705+2552 shows the most distinctive abundance pattern. This star shows strong C, Na, Mg, and Ba enhancements. Given its [Ba/Fe] ratio of 0.67 dex, which is close to the commonly adopted threshold, we tentatively classify it as a CEMP-s star. As shown in the lower left panel of Figure 6, this star has already completed its FDU phase, and its lithium content is expected to be diluted due to the mixing of lithium-poor interior material. However, more evolved AGB stars can produce Li, Na, and *s*-process elements (A. G. W. Cameron & W. A. Fowler 1971; P. Ventura & F. D'Antona 2011). The most plausible mechanism for this star is mass transfer from an AGB companion in a binary system. This star needs further investigation.

In addition, according to H.-L. Yan et al. (2021), the asteroseismic analysis reveals that most Li-rich giants are in the red clump phase, and their lithium abundances are on average much higher than those of Li-rich RGB stars. Among these four Li-rich stars, the HB star J0554+5253 has the highest lithium abundance, which is consistent with the conclusion of H.-L. Yan et al. (2021). This star may have undergone the helium flash, and this event is postulated as the plausible mechanism responsible for its Li enrichment. However, recent studies (J. Zhang et al. 2021) presented that only He-flash contributes limited Li production, suggesting that additional physical mechanisms are required to trigger abnormal Li enhancement. RGB mergers with a helium white dwarf star (HeWD) may provide a possible Li-rich explanation (X. Zhang et al. 2020). Meanwhile, it remains uncertain whether this mechanism can be applied to the VMP regime.

The atomic diffusion model is considered to be an effective mechanism for enhancing the lithium content of unevolved stars with temperatures between 6900 and 7100 K (C. P. Deliyannis et al. 2002). However, $T_{\rm eff}$ of the turnoff star J0626+6032 falls far outside this range, so the atomic diffusion mechanism is unlikely to be the cause of its lithium enhancement. In addition to lithium, this star shows only a slight normal enhancement of Na, while it does not show any other elemental enhancement. Lithium can be produced by outward shock waves or neutrino processes in supernovae (S. E. Woosley et al. 1990; S. E. Woosley & T. A. Weaver 1995), while the production of lithium in Type II supernova explosions is usually accompanied by strong α-element enhancements. In binary systems, stars can increase their surface lithium content by accreting material from a companion star, especially when the companion is a red giant, AGB star, or nova. Another possible mechanism is the accretion of circumstellar material rich in lithium, which could be ejected by the nova explosion (T. Matsuno et al. 2025).

5. Summary

In this paper, we present a homogeneous NLTE abundance analysis of lithium for 103 very metal-poor stars with metallicity down to −4.3 dex. The sample was selected from the LAMOST survey and observed by the high-resolution spectroscopy of Subaru. The stellar parameters were determined using NLTE line formation calculations for Fe I and Fe II. Based on our data, we present new insight into the lithium abundances and lithium plateaus in VMP/EMP stars.

(1) The Spite plateau lies at ∼2.3 dex for warm halo stars. However, it may not be strictly flat, showing a slight positive slope. Most significantly, it appears to extend to lower metallicities as previously suggested, calling into question the reality of the so-called "meltdown" at low metallicity. The classic Spite plateau stars and the stars in the meltdown region have a similar positive slope, indicating a metallicity-extended Spite plateau.

(2) The lithium plateau in LRGB stars was reported by previous work. We confirm that LRGB have a mean lithium abundance of A(Li) = 1.13 dex, which is consistent with previous findings.

(3) The lithium abundance rapidly drops from A(Li) $\sim$ 1.0 to A(Li) < 0.5 as stars evolve from LRGB to highly evolved RGB stars. This may reflect the natural evolutionary continuation of lithium depletion from the Spite plateau through the LRGB phase and into the highly evolved RGB stage under sustained, extra mixing.

(4) We report that the upper limit of the lithium abundance in HB stars is possibly higher than that in highly evolved RGB stars.

(5) We identify four Li-rich stars in our sample across different evolutionary stages, showing complex and multiple Li production mechanisms.

Our results suggest that the observed lithium abundances in VMP/EMP stars result from a complex interplay between depletion and production processes.

Acknowledgments

This work was supported by the National Natural Science Foundation of China under grant No. 12588202, the National Key R&D Programs of China No. 2024YFA1611903, the Strategic Priority Research Program of Chinese Academy of Sciences under grant No. XDB1160101, and the International Partnership Program of Chinese Academy of Sciences under grant No. 178GJHZ2022040GC. This work was also supported by the National Natural Science Foundation of China under grant Nos. 12222305, 12373036, and 12273055. H.Y. and H.L. acknowledge support from the Youth Innovation Promotion Association of the CAS. S.A. acknowledges support from the National Natural Science Foundation of China grant No. W2432009. W.A. was supported by JSPS KAKENHI grant Nos. 21H04499 and 25K01046. This research is based on data collected at Subaru Telescope, which is operated by the National Astronomical Observatory of Japan. We are honored and grateful for the opportunity of observing the Universe from Maunakea, which has cultural, historical, and natural significance in Hawaii. The Guoshoujing Telescope (the Large Sky Area Multi-Object Fiber Spectroscopic Telescope, hereafter LAMOST) is a National Major Scientific Project built by the Chinese Academy of Sciences. LAMOST is operated and managed by the National Astronomical Observatories, Chinese Academy of Sciences. We thank the anonymous referee for the constructive comments, which improved the scientific accuracy and completeness of this work.

Facilities: Subaru (HDS), LAMOST.

Appendix
Results of Program Stars

In this Appendix, we show the detailed results of our sample stars. The results of Li abundance obtained from both LTE and NLTE analysis are listed in Table A1. The stellar parameters and elemental abundances of four Li-rich stars in our sample are shown in Table A2.

Table A1
Li Abundance and Stellar Parameters

Star	$T_{\rm eff}$ (K)	log g (dex)	[Fe/H]	ξ_t (km s^{-1})	A(Li)$_{\rm LTE}$	A(Li)$_{\rm NLTE}$	Phase
J0055 + 1857	5018	2.69	−2.26	1.40	0.94	0.97	2
J0119 + 2425	6412	4.27	−2.57	1.64	2.18	2.17	1
J0131 + 4800	6100	4.03	−1.79	1.35	2.21	2.23	1
J0232 + 0545	6091	3.95	−2.16	1.11	2.34	2.35	1
J0244 + 0828	6472	4.39	−2.27	1.60	2.48	2.47	1
J0246 + 2643	6062	2.71	−2.38	3.30	1.44	1.47[d]	4
J0326 + 0202	4827	1.92	−3.05	1.52	0.85	0.88	3
J0352 + 0514	5859	4.32	−3.11	1.20	1.99	1.99	1
J0423 + 0538	6100	4.12	−2.04	1.31	2.33	2.34	1
J0554 + 5235	5596	2.21	−1.93	2.30	4.04	3.72[c]	4
J0626 + 6032	5926	3.77	−2.20	1.30	3.72	3.54[c]	1
J0637 + 4308	6366	4.11	−2.60	1.55	2.34	2.34	1
J0643 + 5111	5354	3.31	−2.41	1.23	1.44	1.46	2
J0643 + 5934	4877	1.99	−2.46	1.51	0.99	1.03	3
J0705 + 2552[a]	5307	3.09	−3.11	1.42	3.94	3.34[c]	2
J0714 + 1600	5082	2.35	−2.22	1.52	2.32	2.34[c]	2
J0748 + 4613	4645	1.40	−3.03	2.20	0.20	0.23[d]	3
J0828 + 0037	6104	3.48	−2.06	1.65	2.29	2.31	1
J0832 + 2450	6161	3.92	−2.25	1.50	2.20	2.20	1
J0834 + 2307	5261	3.09	−2.63	1.38	1.42	1.43	2
J0845 + 0150	6310	4.01	−2.22	1.75	2.41	2.41	1
J0913 + 0726	6094	4.44	−1.93	1.34	2.36	2.36	1
J0924 + 2651	6201	3.98	−2.47	1.50	2.00	1.99	1
J0934 − 0108	5045	2.25	−2.37	1.49	1.03	1.07	2
J0934 − 0259	5995	4.18	−1.82	1.30	2.24	2.22	1
J1014 + 0547	6051	3.75	−1.68	1.31	2.32	2.35	1
J1017 + 3755	5229	2.58	−2.78	1.51	0.87	1.27	2
J1032 + 4209	4900	1.88	−2.44	1.60	1.10	1.14	3
J1044 − 0358[a]	6319	4.02	−2.02	1.66	1.48	1.48	1
J1050 + 2135	6175	4.29	−2.26	1.27	2.27	2.25	1
J1058 + 0138[a]	6198	3.84	−1.97	1.26	1.58	1.59	1

Table A1
(Continued)

Star	$T_{\rm eff}$ (K)	log g (dex)	[Fe/H]	ξ_t (km s^{-1})	A(Li)$_{\rm LTE}$	A(Li)$_{\rm NLTE}$	Phase
J1059 + 0208	5072	2.74	−2.33	1.13	1.17	1.20	2
J1101 + 2031	5241	2.87	−2.48	1.45	0.54	0.57	2
J1102 + 0102	4908	2.10	−2.24	1.53	1.01	1.06	2
J1109 − 0754	4582	1.09	−3.05	1.98	0.12	0.17[d]	3
J1118 − 0650	4585	1.17	−3.31	2.14	−0.06	0.00[d]	3
J1123 + 0937	5979	4.35	−2.49	1.33	2.19	2.18	1
J1123 + 3217	6275	4.45	−1.81	1.18	2.33	2.30	1
J1135 + 3100	6289	4.22	−2.74	1.61	2.31	2.29	1
J1137 + 4413	6241	4.07	−2.08	1.52	2.42	2.43	1
J1144 + 4032	5600	4.17	−2.52	0.79	2.04	2.03	1
J1147 + 4458	5668	4.36	−2.56	0.56	1.90	1.89	1
J1158 + 0531	5605	3.51	−2.23	1.39	2.12	2.14	1
J1207 + 2244	4743	1.80	−2.78	1.88	0.22	0.25[d]	3
J1210 + 0023	6033	4.38	−2.08	1.00	2.25	2.24	1
J1216 − 0244	6104	4.40	−1.95	1.06	2.43	2.43	1
J1221 + 0907	5081	2.63	−2.35	1.40	1.00	1.03	2
J1225 − 0452	4872	1.90	−2.5	1.92	1.00	1.05	3
J1226 + 2323	4911	1.62	−2.39	1.94	0.26	0.31[d]	3
J1228 + 2519	6212	4.05	−1.84	1.37	2.37	2.38	1
J1231 + 1232	6259	3.93	−2.31	0.85	2.23	2.24	1
J1231 + 5243	5755	3.67	−1.96	1.38	2.32	2.34	1
J1234 + 4201	6118	4.02	−1.98	1.34	2.27	2.28	1
J1237 + 1922	4928	1.65	−2.96	1.95	0.08	0.13[d]	3
J1253 + 0753	6100	4.20	−3.68	1.08	2.07	2.07	1
J1305 + 2815	6072	3.96	−2.81	1.52	2.12	2.12	1
J1313 − 0552[b]	4550	1.76	−4.32	2.02	0.08	0.15[d]	3
J1345 + 0513	4614	1.17	−2.59	2.09	1.16	1.19	3
J1350 + 0819	6140	4.00	−2.33	1.70	2.34	2.34	1
J1352 + 2646	4780	1.63	−2.77	1.50	0.21	0.23[d]	3
J1353 + 2021	5959	4.25	−2.75	1.34	2.02	2.02	1
J1359 + 2112[a]	6264	3.83	−2.13	1.65	1.86	1.87	1
J1401 + 2659	6001	3.88	−2.89	1.50	2.03	2.04	1
J1404 + 3222	6252	3.81	−1.93	1.54	2.32	2.33	1
J1404 + 4111	6159	3.97	−1.83	1.35	2.32	2.33	1
J1410 − 0555[b]	6405	4.23	−3.06	1.30	2.41	2.40	1
J1414 + 1457	4707	1.14	−2.50	2.01	0.23	0.27[d]	3
J1414 + 1721	4945	2.25	−2.49	1.50	1.06	1.09	2
J1423 + 0322	4540	1.05	−2.75	2.18	−0.05	−0.02[d]	3
J1424 + 3343	5971	4.11	−1.88	1.25	2.22	2.24	1
J1432 + 3755	4585	1.34	−3.13	2.08	0.16	0.19[d]	3
J1434 + 3540[a]	5876	4.17	−1.83	1.21	1.57	1.59	1
J1456 + 3122	4770	1.76	−2.78	1.63	0.74	0.77	3
J1459 + 0444	4675	1.40	−2.65	2.00	0.00	0.03[d]	3
J1518 + 2544	5417	1.90	−2.04	2.16	0.76	0.84[d]	4
J1523 + 0714	4550	0.51	−2.57	2.07	0.10	0.13[d]	3
J1541 + 3009	6152	4.04	−1.72	1.21	2.38	2.38	1
J1548 + 2113	5140	2.75	−2.26	1.46	1.04	1.08	2
J1558 + 4149	6356	4.11	−1.83	1.33	2.48	2.49	1
J1629 + 1430	4590	1.47	−3.20	2.30	0.15	0.18[d]	3
J1634 + 0206	5247	1.91	−2.02	1.72	0.93	0.99[d]	4
J1640 + 1550	4580	0.90	−2.89	2.34	0.18	0.21[d]	3
J1657 + 3443	4770	1.60	−2.73	1.50	0.75	0.78	3
J1700 + 2159	5517	2.33	−2.48	2.06	1.07	1.13[d]	4
J1718 + 5044	5385	2.06	−2.48	2.16	0.90	0.96[d]	4
J1730 + 4143	4700	1.36	−2.56	1.60	0.89	0.93	3
J1731 + 2843	5017	2.45	−2.09	1.40	1.11	1.16	2
J1733 + 2633	5013	2.55	−3.24	1.60	0.91	0.94	2
J1829 + 4852	6213	4.16	−1.98	1.26	2.36	2.35	1
J1833 + 1309	5362	3.14	−2.45	1.15	1.60	1.62	2
J1954 + 5853	5992	3.52	−1.90	1.64	2.35	2.37	1
J1958 + 5533	6286	4.02	−2.20	1.73	2.37	2.36	1
J2109 + 1725	4807	1.73	−2.62	1.68	0.83	0.87	3

Table A1
(Continued)

Star	$T_{\rm eff}$ (K)	log g (dex)	[Fe/H]	ξ_t (km s^{-1})	A(Li)$_{\rm LTE}$	A(Li)$_{\rm NLTE}$	Phase
J2216 + 0246	4784	2.06	−2.33	1.90	0.64	0.68	3
J2216 + 2232	4681	1.40	−2.79	1.77	0.76	0.79	3
J2217 + 2104[b]	4507	1.21	−3.82	2.40	−0.07	−0.01[d]	3
J2221 + 0228	5219	2.86	−2.99	1.55	1.16	1.19	2
J2242 + 2720	4698	1.58	−3.59	2.11	−0.01	0.06[d]	3
J2347 + 2851	4731	1.30	−2.33	1.81	0.09	0.12[d]	3
J2350 + 0236	6171	4.18	−2.92	1.60	2.19	2.19	1

Notes. Phases: (1) unevolve stars, (2) RGB stars, (3) highly evolved stars, and (4) horizontal branch.
[a] CEMP-s.
[b] CEMP-no.
[c] Average of 6707.8 and 6103.6 Å.
[d] Upper limit of A(Li).

Table A2
Stellar Parameters and Elemental Abundances of Li-rich Stars

Stellar Parameters	J0554 +5235	J0626 +6032	J0705 +2552	J0714 +1600
$T_{\rm eff}$(K)	5596	5926	5307	5082
log g(dex)	2.21	3.77	3.09	2.35
[Fe/H]	−1.93	−2.20	−3.11	−2.22
ξ_t(km s^{-1})	2.30	1.30	1.42	1.52
Elemental abundances				
A(Li)$_{\rm NLTE}$	3.72	3.54	3.34	2.34
[C/Fe]$_{\rm NLTE}$	0.09	0.02	1.47	−0.09
[Na/Fe]$_{\rm NLTE}$	0.05	0.38	1.37	…
[Mg/Fe]$_{\rm NLTE}$	0.47	0.26	1.11	0.40
[Ca/Fe]$_{\rm NLTE}$	0.36	…	0.60	…
[Sc/Fe]$_{\rm NLTE}$	−0.08	0.09	0.41	…
[Ba/Fe]$_{\rm NLTE}$	−0.01	0.26	0.67	…
[Eu/Fe]$_{\rm NLTE}$	0.85	0.30	0.30	…

ORCID iDs

Hong-Liang Yan https://orcid.org/0000-0002-8609-3599
Jinxiao Qin https://orcid.org/0009-0000-2934-4067
Shuai Liu https://orcid.org/0000-0001-5193-1727
Zeming Zhou https://orcid.org/0000-0002-1619-1660
Gang Zhao https://orcid.org/0000-0002-8980-945X
Jianrong Shi https://orcid.org/0000-0002-0349-7839
Sofya Alexeeva https://orcid.org/0000-0002-8709-4665
Huawei Zhang https://orcid.org/0000-0002-7727-1699
Haining Li https://orcid.org/0000-0002-0389-9264
Huiling Chen https://orcid.org/0009-0008-2988-2680
Junbo Zhang https://orcid.org/0000-0002-3395-6178
Yufu Shen https://orcid.org/0000-0003-4445-6504
Wako Aoki https://orcid.org/0000-0002-8975-6829
Tadafumi Matsuno https://orcid.org/0000-0002-8077-4617
Jingkun Zhao https://orcid.org/0000-0003-2868-8276

References

Aguado, D. S., González Hernández, J. I., Allende Prieto, C., & Rebolo, R. 2019, ApJL, 874, L21
Aguilera-Gómez, C., Chanamé, J., Pinsonneault, M. H., & Carlberg, J. K. 2016, ApJL, 833, L24
Alexander, J. B. 1967, Obs, 87, 238
Alexeeva, S., Ryabchikova, T., Mashonkina, L., & Hu, S. 2018, ApJ, 866, 153
Alexeeva, S., Wang, Y., Zhao, G., et al. 2023, ApJ, 957, 10
Alexeeva, S. A., Pakhomov, Y. V., & Mashonkina, L. I. 2014, AstL, 40, 406
Amarsi, A. M., Lind, K., Asplund, M., Barklem, P. S., & Collet, R. 2016, MNRAS, 463, 1518
Aoki, W., Barklem, P. S., Beers, T. C., et al. 2009, ApJ, 698, 1803
Aoki, W., Li, H., Matsuno, T., et al. 2022, ApJ, 931, 146
Aoki, W., Matsuno, T., Honda, S., et al. 2018, PASJ, 70, 94
Arai, A., Tajitsu, A., Kawakita, H., & Shinnaka, Y. 2021, ApJ, 916, 44
Arnould, M., & Norgaard, H. 1975, A&A, 42, 55
Ashwell, J. F., Jeffries, R. D., Smalley, B., et al. 2005, ESASP, 560, 403
Asplund, M. 2005, ARA&A, 43, 481
Asplund, M., Amarsi, A. M., & Grevesse, N. 2021, A&A, 653, A141
Bandyopadhyay, A., Sivarani, T., Beers, T. C., et al. 2022, ApJ, 937, 52
Barklem, P. S., O'Mara, B. J., & Ross, J. E. 1998, MNRAS, 296, 1057
Beers, T. C., & Christlieb, N. 2005, ARA&A, 43, 531
Bonifacio, P., Caffau, E., François, P., & Spite, M. 2025, A&ARv, 33, 2
Bonifacio, P., Caffau, E., Spite, M., et al. 2018, A&A, 612, A65
Bonifacio, P., & Molaro, P. 1997, MNRAS, 285, 847
Bonifacio, P., Molaro, P., Sivarani, T., et al. 2007, A&A, 462, 851
Borisov, S., Prantzos, N., & Charbonnel, C. 2024, A&A, 691, A142
Caffau, E., Steffen, M., Molaro, P., et al. 2025, A&A, 704, A238
Cameron, A. G. W., & Fowler, W. A. 1971, ApJ, 164, 111
Cayrel, R., Depagne, E., Spite, M., et al. 2004, A&A, 416, 1117
Charbonnel, C., & Prantzos, N. 2026, arXiv:2602.17470
Christlieb, N., Bessell, M. S., Beers, T. C., et al. 2002, Natur, 419, 904
Coc, A., Vangioni-Flam, E., Descouvemont, P., Adahchour, A., & Angulo, C. 2004, ApJ, 600, 544
Cohen, J. G., Christlieb, N., Thompson, I., et al. 2013, ApJ, 778, 56
Cooke, R. J., Pettini, M., & Steidel, C. C. 2018, ApJ, 855, 102
Cui, X.-Q., Zhao, Y.-H., Chu, Y.-Q., et al. 2012, RAA, 12, 1197
Cyburt, R. H., Fields, B. D., Olive, K. A., & Yeh, T.-H. 2016, RvMP, 88, 015004
Deliyannis, C. P., Demarque, P., & Kawaler, S. D. 1990, ApJS, 73, 21
Deliyannis, C. P., Steinhauer, A., & Jeffries, R. D. 2002, ApJL, 577, L39
Denissenkov, P. A., Truran, J. W., Pignatari, M., et al. 2014, MNRAS, 442, 2058
Ezzeddine, R., Frebel, A., & Plez, B. 2017, ApJ, 847, 142
Fields, B. D., Daigne, F., Cassé, M., & Vangioni-Flam, E. 2002, ApJ, 581, 389
François, P., Wanajo, S., Caffau, E., et al. 2020, A&A, 642, A25
Frebel, A., & Norris, J. E. 2015, ARA&A, 53, 631
Fu, X., Bressan, A., Molaro, P., & Marigo, P. 2015, MNRAS, 452, 3256
Gao, J., Zhu, C., Lü, G., et al. 2024, ApJ, 971, 4
Gehren, T., Liang, Y. C., Shi, J. R., Zhang, H. W., & Zhao, G. 2004, A&A, 413, 1045
Ghezzi, L., Montet, B. T., & Johnson, J. A. 2018, ApJ, 860, 109
Grisoni, V., Matteucci, F., Romano, D., & Fu, X. 2019, MNRAS, 489, 3539
Guandalini, R., Palmerini, S., Busso, M., & Uttenthaler, S. 2009, PASA, 26, 168
Gustafsson, B., Edvardsson, B., Eriksson, K., et al. 2008, A&A, 486, 951
Gutiérrez, C. M., García López, R. J., Rebolo, R., Martín, E. L., & François, P. 1999, A&AS, 137, 93
Hansen, T., Hansen, C. J., Christlieb, N., et al. 2014, ApJ, 787, 162

Hartwig, T., Ishigaki, M. N., Klessen, R. S., & Yoshida, N. 2019, MNRAS, 482, 1204
Helmi, A., Babusiaux, C., Koppelman, H. H., et al. 2018, Natur, 563, 85
Hernanz, M., Jose, J., Coc, A., & Isern, J. 1996, ApJL, 465, L27
Hosford, A., Ryan, S. G., García Pérez, A. E., Norris, J. E., & Olive, K. A. 2009, A&A, 493, 601
Iocco, F., Mangano, G., Miele, G., Pisanti, O., & Serpico, P. D. 2009, PhR, 472, 1
Izzo, L., Della Valle, M., Mason, E., et al. 2015, ApJL, 808, L14
José, J., & Hernanz, M. 1998, ApJ, 494, 680
Kemp, A. J., Karakas, A. I., Casey, A. R., et al. 2022, ApJL, 933, L30
Kielty, C. L., Venn, K. A., Sestito, F., et al. 2021, MNRAS, 506, 1438
Kobayashi, C., Leung, S.-C., & Nomoto, K. 2020, ApJ, 895, 138
Koch, A., Lind, K., & Rich, R. M. 2011, ApJL, 738, L29
Lagarde, N., Reylé, C., Robin, A. C., et al. 2019, A&A, 621, A24
Lemoine, M., Vangioni-Flam, E., & Cassé, M. 1998, ApJ, 499, 735
Li, H., Aoki, W., Matsuno, T., et al. 2018, ApJL, 852, L31
Li, H., Aoki, W., Matsuno, T., et al. 2022, ApJ, 931, 147
Li, L.-J., & Qian, S.-B. 2014, MNRAS, 444, 600
Lind, K., Bergemann, M., & Asplund, M. 2012, MNRAS, 427, 50
Lind, K., Primas, F., Charbonnel, C., Grundahl, F., & Asplund, M. 2009, A&A, 503, 545
Martín, E. 2023, Lithium Across the Universe (IOP Publishing)
Mashonkina, L., Gehren, T., Shi, J. R., Korn, A. J., & Grupp, F. 2011, A&A, 528, A87
Mashonkina, L., Jablonka, P., Pakhomov, Y., Sitnova, T., & North, P. 2017a, A&A, 604, A129
Mashonkina, L., Jablonka, P., Sitnova, T., Pakhomov, Y., & North, P. 2017b, A&A, 608, A89
Matas Pinto, A. M., Spite, M., Caffau, E., et al. 2021, A&A, 654, A170
Matsuno, T., Aoki, W., Beers, T. C., Lee, Y. S., & Honda, S. 2017, AJ, 154, 52
Matsuno, T., Kemp, A., Tanikawa, A., et al. 2025, A&A, 699, A171
Meléndez, J., Casagrande, L., Ramírez, I., Asplund, M., & Schuster, W. J. 2010, A&A, 515, L3
Meléndez, J., & Ramírez, I. 2004, ApJL, 615, L33
Molaro, P., Bonifacio, P., Cupani, G., & Howk, J. C. 2024, A&A, 690, A38
Molaro, P., Cescutti, G., & Fu, X. 2020, MNRAS, 496, 2902
Molaro, P., Izzo, L., D'Odorico, V., et al. 2022, MNRAS, 509, 3258
Molaro, P., Izzo, L., Mason, E., Bonifacio, P., & Della Valle, M. 2016, MNRAS, 463, L117
Monaco, L., Bonifacio, P., Sbordone, L., Villanova, S., & Pancino, E. 2010, A&A, 519, L3
Monaco, L., Caffau, E., Molaro, P., Bonifacio, P., & Cescutti, G. 2025, A&A, 697, A75
Mucciarelli, A., Bonifacio, P., Monaco, L., Salaris, M., & Matteuzzi, M. 2024, A&A, 689, A89
Mucciarelli, A., Monaco, L., Bonifacio, P., et al. 2022, A&A, 661, A153
Mucciarelli, A., Salaris, M., & Bonifacio, P. 2012, MNRAS, 419, 2195
Myeong, G. C., Evans, N. W., Belokurov, V., Amorisco, N. C., & Koposov, S. E. 2018, MNRAS, 475, 1537
Nakamura, K., & Shigeyama, T. 2004, ApJ, 610, 888
Nomoto, K., Kobayashi, C., & Tominaga, N. 2013, ARA&A, 51, 457
Nordlander, T., Amarsi, A. M., Lind, K., et al. 2017, A&A, 597, A6
Palmerini, S., Cristallo, S., Busso, M., et al. 2011, ApJ, 741, 26
Planck Collaboration, Aghanim, N., Ashdown, M., et al. 2016, A&A, 596, A109
Prantzos, N. 2012, A&A, 542, A67
Rebolo, R., Beckman, J., & Molaro, P. 1987, A&A, 172, L17
Reetz, J. 1999, PhD thesis, Ludwig-Maximilians-Universität München
Roederer, I. U., Preston, G. W., Thompson, I. B., Shectman, S. A., & Sneden, C. 2014, ApJ, 784, 158
Romano, D., Karakas, A. I., Tosi, M., & Matteucci, F. 2010, A&A, 522, A32
Romano, D., Magrini, L., Randich, S., et al. 2021, A&A, 653, A72
Ryan, S. G., Beers, T. C., Olive, K. A., Fields, B. D., & Norris, J. E. 2000, ApJL, 530, L57
Ryan, S. G., Norris, J. E., & Beers, T. C. 1999, ApJ, 523, 654
Rybicki, G. B., & Hummer, D. G. 1991, A&A, 245, 171
Rybicki, G. B., & Hummer, D. G. 1992, A&A, 262, 209
Sackmann, I.-J., & Boothroyd, A. I. 1999, ApJ, 510, 217
Sbordone, L., Bonifacio, P., Caffau, E., et al. 2010, A&A, 522, A26
Schaeuble, M., & King, J. R. 2012, PASP, 124, 164
Selvelli, P., Molaro, P., & Izzo, L. 2018, MNRAS, 481, 2261
Shi, J., Zhao, G., Liu, S., et al. 2025, ApJ, 983, 127
Shi, J. R., Gehren, T., Butler, K., Mashonkina, L. I., & Zhao, G. 2008, A&A, 486, 303
Shi, J. R., Gehren, T., Zhang, H. W., Zeng, J. L., & Zhao, G. 2007, A&A, 465, 587
Sitnova, T., Zhao, G., Mashonkina, L., et al. 2015, ApJ, 808, 148
Spite, F., & Spite, M. 1982a, A&A, 115, 357
Spite, M., & Spite, F. 1982b, Natur, 297, 483
Starrfield, S., Bose, M., Iliadis, C., et al. 2024, ApJ, 962, 191
Starrfield, S., Truran, J. W., Sparks, W. M., & Arnould, M. 1978, ApJ, 222, 600
Tajitsu, A., Sadakane, K., Naito, H., Arai, A., & Aoki, W. 2015, Natur, 518, 381
Ventura, P., & D'Antona, F. 2011, MNRAS, 410, 2760
Wang, E. X., Nordlander, T., Asplund, M., et al. 2021, MNRAS, 500, 2159
Woosley, S. E., Hartmann, D. H., Hoffman, R. D., & Haxton, W. C. 1990, ApJ, 356, 272
Woosley, S. E., & Weaver, T. A. 1995, ApJS, 101, 181
Yan, H., Li, H., Wang, S., et al. 2022, Innov, 3, 100224
Yan, H. L., Shi, J. R., & Zhao, G. 2015, ApJ, 802, 36
Yan, H.-L., Shi, J.-R., Zhou, Y.-T., et al. 2018, NatAs, 2, 790
Yan, H.-L., Zhou, Y.-T., Zhang, X., et al. 2021, NatAs, 5, 86
Yi, S. K., demarque, P., & Kim, Y.-C. 2004, Ap&SS, 291, 261
Zhang, H. W., Gehren, T., Butler, K., Shi, J. R., & Zhao, G. 2006, A&A, 457, 645
Zhang, H. W., Gehren, T., & Zhao, G. 2008, A&A, 481, 489
Zhang, H.-W., & Zhao, G. 2003, ChJAA, 3, 453
Zhang, J., Shi, J.-R., Yan, H.-L., et al. 2021, ApJL, 919, L3
Zhang, R., Matsuno, T., Li, H., et al. 2024, ApJ, 966, 174
Zhang, X., Jeffery, C. S., Li, Y., & Bi, S. 2020, ApJ, 889, 33
Zhao, G., Butler, K., & Gehren, T. 1998, A&A, 333, 219
Zhao, G., & Gehren, T. 2000, A&A, 362, 1077
Zhao, G., Mashonkina, L., Yan, H. L., et al. 2016, ApJ, 833, 225
Zhao, G., Zhao, Y.-H., Chu, Y.-Q., Jing, Y.-P., & Deng, L.-C. 2012, RAA, 12, 723